Inorganic Chemistry

Article

pubs.acs.org/IC

Lanthanide Coordination Polymers with "fsy-type" Topology Based on 4,4′-Azobenzoic Acid: Syntheses, Crystal Structures, and Magnetic Properties

Shaowei Zhang, Wei Shi,* Leilei Li, Eryue Duan, and Peng Cheng*

Department of Chemistry, Key Laboratory of Advanced Energy Materials Chemistry (MOE), and Collaborative Innovation Center of Chemical Science and Engineering, Nankai University, No. 94, Weijin Road, Tianjin 300071, P. R. China

Supporting Information

ABSTRACT: Seven lanthanide coordination polymers (CPs), $[Ln_2(azdc)_3(DMA)_2]_n \cdot 2n(DMA)$ (Ln = Sm^{III} for **1**, Eu^{III} for **2**, Gd^{III} for **3**, Tb^{III} for **4**, Dy^{III} for **5**, Ho^{III} for **6**, Er^{III} for **7**; H_2azdc = 4,4′-azobenzoic acid, DMA = *N*,*N*-dimethylacetamide), have been successfully prepared with high yields via solvothermal methods and further studied by elemental analyses (EA), powder X-ray diffraction (PXRD), UV−vis spectra, photoluminescent spectra, thermogravimetric analyses (TGA), variable-temperature in situ PXRD analyses, and single-crystal X-ray diffraction. CPs **1**−**7** all consist of unique 1D lanthanide-carboxylate building units $[Ln_2(CO_2)_6]_n$ constructed from the adjacent Ln^{III} cations and carboxyl groups of the H_2azdc ligands, which can further generate 3D frameworks with "fsy"-type topological structures via the link of $azdc^{2-}$. Furthermore, variable-temperature magnetic susceptibility measurements of **1**−**7** have been investigated. The results indicate that unusual ferromagnetic coupling between adjacent Gd^{III} cations exists in **3**, which is rarely reported in the Gd^{III} complexes only bridged by $\mu_{1,3}$-COO groups. Meanwhile, the magnetic study reveals that **3** displays cryogenic magnetic refrigeration property, whereas **5** shows magnetic dynamics at low temperature.

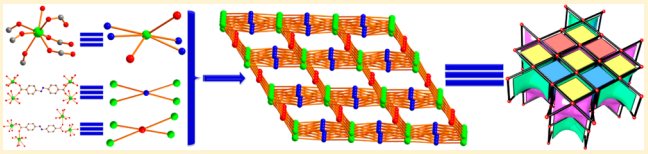

INTRODUCTION

The ongoing studies for novel lanthanide-containing coordination polymers (Ln-CPs) have currently provoked predominant attentions for the past two decades, owing to not only their abundant and various intriguing structures,[1−4] but also their possible applications such as luminescent sensing,[2] magnetism,[3] and magnetic resonance imaging (MRI) contrast agents fields.[4] For photoluminescence in both visible and near-infrared regions, Ln^{III} cations are usually used as luminescent centers for their characteristic narrow line-like emissions for pure colors.[2] For magnetic properties, because of that orbital contribution to the significant magnetic anisotropy, Ln^{III} cations have been widely investigated in the field of molecular magnetism, especially for Tb^{III} and Dy^{III}. For example, single-molecule magnets (SMMs), single-ion magnets (SIMs), and single-chain magnets (SCMs) exhibit slow relaxation of the magnetization at low temperature, providing the promising candidates to make spintronic devices.[3]

In recent years, our group has designed and synthesized series of Ln-CPs with interesting properties including luminescent sensing, magnetism, and gas storage and separation.[5] As a continuation work, in this contribution, H_2azdc was chosen to synthesize Ln-CPs because azobenzene and its derivatives are widely known as photochromic ligands which could sustain clean and efficient invertible photoisomerization for the azo bond between *cis* and *trans* states under irradiation or heating, as well as other conditions (coordinated *trans*, $\lambda_{max} \approx 370$ nm; *cis*, $\lambda_{max} \approx 460$ nm).[6] The introduction of H_2azdc in the formation of CPs has resulted in limited success (Supporting Information Table S1). Though a small number of CPs constructed by transition metal (TM) or main group elements and H_2azdc ligands have been synthesized to date,[7] the investigations on Ln-CPs with H_2azdc ligands are very rare.[1c,2d,8] Yaghi's group isolated the extended 3D framework MOF-9, $[Tb_2(azdc)_3(DMSO)_4 \cdot 16(DMSO)]_n$, by diffusion methods in 2000.[1c] In 2010, four isomorphous CPs of MOF-9, $[Ln_2(azdc)_3(DMSO)_4 \cdot 6(DMSO) \cdot 8(H_2O)]_n$ (Ln = Ce^{III}, Sm^{III}, Eu^{III}, Gd^{III}), as well as the other two porous CPs, $[Ce_3(azdc)_3(Hazdc)_3 \cdot 30(DMSO) \cdot 29(H_2O)]_n$, and $[Ce_2(azdc)_3(H_2O)_3]_n$, were synthesized by You et al.[2d] In addition, two 3D pillared-layer CPs with mixed ligands, $Ln_2(\mu_3\text{-}OH)(azdc)_{1.5}(C_2O_4)$ (Ln = Sm^{III}, Eu^{III}), were documented by Cao's group in the same year.[8]

Herein, a family of 3D Ln-CPs, $[Ln_2(azdc)_3(DMA)_2]_n \cdot 2n(DMA)$ [Ln = Sm^{III} for **1**, Eu^{III} for **2**, Gd^{III} for **3**, Tb^{III} for **4**, Dy^{III} for **5**, Ho^{III} for **6**, Er^{III} for **7**], have been successfully obtained by solvothermal method. CPs **1**−**7** all consist of 1D Ln-carboxylate building units $[Ln_2(CO_2)_6]_n$, which can further produce 3D (4, 4, 6)-net framework with the Schläfli symbol of $\{4^2 \cdot 8^4\}\{4^4 \cdot 6^2\}_2\ \{4^8 \cdot 6^6 \cdot 8\}_2$. Moreover, the magnetic properties of **1**−**7** have also been studied.

EXPERIMENTAL SECTION

General Methods and Materials. The salts $LnCl_3 \cdot 6H_2O$ (Ln = Sm, Eu, Gd, Tb, Dy, Ho, Er) were obtained by dissolving Ln_2O_3 or

Received: June 13, 2014
Published: September 5, 2014

   dx.doi.org/10.1021/ic501395p | *Inorg. Chem.* 2014, 53, 10340−10346

Table 1. Crystallographic Data and Structure Refinements for 1−7

	1	2	3	4	5	6	7
formula	$C_{58}H_{60}N_{10}O_{16}Sm_2$	$C_{58}H_{60}N_{10}O_{16}Eu_2$	$C_{58}H_{60}N_{10}O_{16}Gd_2$	$C_{58}H_{60}N_{10}O_{16}Tb_2$	$C_{58}H_{60}N_{10}O_{16}Dy_2$	$C_{58}H_{60}N_{10}O_{16}Ho_2$	$C_{58}H_{60}N_{10}O_{16}Er_2$
M_r (g mol^{-1})	1453.87	1457.08	1467.65	1471.01	1478.15	1483.02	1487.67
T (K)	127	127	127	127	127	127	127
cryst syst	monoclinic	monoclinic	monoclinic	monoclinic	monoclinic	monoclinic	monoclinic
space group	$P2_1/n$	$P2_1/n$	$P2_1/n$	$P2_1/n$	$P2_1/n$	$P2_1/n$	$P2_1/n$
a (Å)	16.2954(5)	16.2499(5)	16.2318(5)	16.2538(5)	16.2078(5)	16.1925(5)	16.1705(5)
b (Å)	8.7619(3)	8.7451(3)	8.7252(3)	8.7093(3)	8.7082(3)	8.6926(3)	8.6943(3)
c (Å)	20.7550(6)	20.7317(6)	20.7773(6)	20.8595(6)	20.8775(6)	20.8815(6)	20.8797(6)
β (deg)	95.316(3)	95.213(3)	94.984(3)	94.891(3)	94.748(3)	94.797(3)	94.633(3)
V (Å^3)	2950.64(16)	2933.93(16)	2931.47(16)	2942.11(16)	2936.54(16)	2928.87(16)	2925.93(16)
Z	2	2	2	2	2	2	2
cryst size (mm^3)	0.18 × 0.14 × 0.10	0.18 × 0.12 × 0.06	0.16 × 0.12 × 0.06	0.18 × 0.12 × 0.06	0.14 × 0.12 × 0.06	0.16 × 0.12 × 0.06	0.12 × 0.10 × 0.06
D_c (g cm^{-3})	1.538	1.551	1.564	1.562	1.573	1.583	1.590
μ (mm^{-1})	2.041	2.189	2.314	2.455	2.596	2.753	2.920
R_{int}	0.0530	0.0443	0.0354	0.0427	0.0680	0.0343	0.0386
limiting indices	$-19 \le h \le 11$	$-18 \le h \le 19$	$-19 \le h \le 17$	$-19 \le h \le 17$	$-18 \le h \le 19$	$-7 \le h \le 19$	$-19 \le h \le 19$
	$-10 \le k \le 8$	$-10 \le k \le 10$	$-10 \le k \le 10$	$-9 \le k \le 10$	$-10 \le k \le 6$	$-10 \le k \le 9$	$-10 \le k \le 9$
	$-24 \le l \le 24$	$-24 \le l \le 22$	$-24 \le l \le 24$	$-24 \le l \le 24$	$-24 \le l \le 21$	$-24 \le l \le 24$	$-24 \le l \le 23$
reflns collected	12 786	11 560	12 730	13 296	12 681	12 160	11 861
indep reflns	5182	5153	5100	5160	5145	5143	5141
params	409	409	409	394	409	394	403
GOF on F^2	1.035	1.058	1.051	1.038	1.037	1.054	1.080
R1, wR2 [$I > 2\sigma(I)$]	0.0479, 0.1168	0.0491, 0.1148	0.0399, 0.0887	0.0473, 0.1143	0.0502, 0.1069	0.0449, 0.1047	0.0448, 0.1010
R1, wR2 (all data)	0.0575, 0.1247	0.0630, 0.1246	0.0477, 0.0933	0.0579, 0.1223	0.0713, 0.1194	0.0538, 0.1104	0.0513, 0.1055

Ln_4O_7 in an aqueous solution of HCl and evaporated slowly. H_2azdc was synthesized according to the literature[9] and further confirmed by ^{1}H NMR. Other chemical reagents were all purchased and used as they were. Elemental analyses (C, H, and N) were measured on a Perkin Elmer 2400-II CHNS/O analyzer. Thermogravimetric analyses (TGA) were obtained under a N_2 atmosphere on a Labsys NETZSCH TG 209 Setaram apparatus with the heating rate of 10 °C min^{-1} from 25 to 800 °C. UV−vis spectra were performed on a JASCO V-570 spectrophotometer at room temperature. The photoluminescent spectra were recorded on a Varian Cary Eclipse fluorescence spectrophotometer. PXRD data were examined on a Rigaku Ultima IV instrument with Cu Kα radiation (λ = 1.540 56 Å), with a scan speed of 10° min^{-1} in the range 2θ = 3−60°. The variable-temperature in situ PXRD pattern was examined on the Pt sample platform under N_2 atmosphere with the heating rate 10 °C min^{-1} from 25 to 550 °C, with a scan speed of 5° min^{-1} in the range 2θ = 3−35°. Magnetic data were obtained using a Quantum Design SQUID VSM magnetometer. Diamagnetic corrections were made with both Pascal's constants and sample holder. The ^{1}H NMR spectrum was tested on a Mercury Vx-300 NMR spectrometer.

*Synthesis of [Sm_2(azdc)$_3$(DMA)$_2$]$_n$·2n(DMA) (**1**).* A mixture of $SmCl_3·6H_2O$ (0.0365 g, 0.10 mmol), H_2azdc (0.027 g, 0.10 mmol), and DMA (5 mL) was magnetically stirred for 10 min. The resulting mixture was transferred into a 25 mL Telfon-lined stainless steel autoclave, kept at 160 °C for 72 h, and then slowly cooled to ambient temperature in 48 h. Orange strip crystals were collected by filtering, washed with DMA, and dried in air. Yield: ca. 86% (based on H_2azdc). The amount of solvent molecules contained in the crystal was determined by elemental analyses and TGA results. Anal. Calcd (%) for $C_{58}H_{60}N_{10}O_{16}Sm_2$: C 47.91, H 4.16, N 9.63. Found: C 47.63, H 4.24, N 9.45.

*Synthesis of [Eu_2(azdc)$_3$(DMA)$_2$]$_n$·2n(DMA) (**2**).* The preparation of **2** was similar to that of **1**, except that $EuCl_3·6H_2O$ (0.0366 g, 0.10 mmol) replaced $SmCl_3·6H_2O$. Yield: ca. 85% (based on H_2azdc). Anal. Calcd (%) for $C_{58}H_{60}N_{10}O_{16}Eu_2$: C 47.81, H 4.15, N 9.61. Found: C 47.68, H 4.21, N 9.39.

*Synthesis of [Gd_2(azdc)$_3$(DMA)$_2$]$_n$·2n(DMA) (**3**).* The preparation of **3** was similar to that of **1**, except that $GdCl_3·6H_2O$ (0.0372 g, 0.10 mmol) replaced $SmCl_3·6H_2O$. Yield: ca. 88% (based on H_2azdc). Anal. Calcd (%) for $C_{58}H_{60}N_{10}O_{16}Gd_2$: C 47.46, H 4.12, N 9.54. Found: C 47.41, H 4.23, N 9.30.

*Synthesis of [Tb_2(azdc)$_3$(DMA)$_2$]$_n$·2n(DMA) (**4**).* The preparation of **4** was similar to that of **1**, except that $TbCl_3·6H_2O$ (0.0374 g, 0.10 mmol) replaced $SmCl_3·6H_2O$. Yield: ca. 82% (based on H_2azdc). Anal. Calcd (%) for $C_{58}H_{60}N_{10}O_{16}Tb_2$: C 47.36, H 4.11, N 9.52. Found: C 47.15, H 4.09, N 9.32.

*Synthesis of [Dy_2(azdc)$_3$(DMA)$_2$]$_n$·2n(DMA) (**5**).* The preparation of **5** was similar to that of **1**, except that $DyCl_3·6H_2O$ (0.0377 g, 0.10 mmol) replaced $SmCl_3·6H_2O$. The reaction temperature was kept at 150 °C for 72 h. Yield: ca. 75% (based on H_2azdc). Anal. Calcd (%) for $C_{58}H_{60}N_{10}O_{16}Dy_2$: C 47.13, H 4.10, N 9.48. Found: C 46.94, H 4.11, N 9.29.

*Synthesis of [Ho_2(azdc)$_3$(DMA)$_2$]$_n$·2n(DMA) (**6**).* The preparation of **6** was similar to that of **1**, except that $HoCl_3·6H_2O$ (0.0380 g, 0.10 mmol) replaced $SmCl_3·6H_2O$ and the reaction temperature was kept at 140 °C for 72 h. Yield: ca. 66% (based on H_2azdc). Anal. Calcd (%) for $C_{58}H_{60}N_{10}O_{16}Ho_2$: C 46.97, H 4.08, N 9.44. Found: C 47.04, H 4.11, N 9.46.

*Synthesis of [Er_2(azdc)$_3$(DMA)$_2$]$_n$·2n(DMA) (**7**).* The preparation of **7** was similar to that of **1**, except that $ErCl_3·6H_2O$ (0.0382 g, 0.10 mmol) replaced $SmCl_3·6H_2O$ and the reaction temperature was kept at 120 °C for 72 h. Yield: ca. 48% (based on H_2azdc). Anal. Calcd (%) for $C_{58}H_{60}N_{10}O_{16}Er_2$: C 46.83, H 4.07, N 9.42. Found: C 46.79, H 4.15, N 9.34.

X-ray Crystallography. Crystallographic data of **1**−**7** were collected on an Oxford SuperNova diffractometer with graphite monochromatic Mo Kα radiation (λ = 0.710 73 Å) at 127 K. Routine Lorentz polarization and empirical absorption corrections were applied. All the structures were solved by direct methods and refined by full-matrix least-squares methods on F^2 with the SHELXTL-97 program package.[10] Anisotropic thermal parameters were assigned to all non-hydrogen atoms. Positions of H atoms attached to C and N atoms were geometrically added. The disorder DMA molecules were geometrically restrained. The final formulas were determined through single-crystal structures, element analyses, and TGA. The crystallographic data and structural refinements for **1**−**7** are summarized in

dx.doi.org/10.1021/ic501395p | Inorg. Chem. 2014, 53, 10340−10346

Table 1. CCDC nos. 1000590−1000596 are for **1**−**7**, respectively. These data can be obtained free of charge from The Cambridge Crystallographic Data Centre via www.ccdc.cam.ac.uk/data_request/cif.

RESULTS AND DISCUSSION

Structural Descriptions. The experimental PXRD patterns for **1**−**7** are in good accordance with the simulated PXRD patterns from the data of single-crystal X-ray diffraction, suggesting high phase purity for **1**−**7** (Supporting Information Figure S1). The different intensities between the simulated and experimental PXRD patterns may be ascribed to the variation in preferred orientation of the powder. In addition, bond-valence sum calculations[11] indicate that all Ln atoms in **1**−**7** are in +3 oxidation state, respectively. The Ln−O bond lengths (Supporting Information Table S2) decrease as the ionic radius of the Ln^{III} cations decreases, which originates from the effect of the lanthanide contraction.[12]

X-ray crystallographic analyses reveal that **1**−**7** are isomorphous and crystallize in the monoclinic space group $P2_1/n$. $[Sm_2(azdc)_3(DMA)_2]_n{\cdot}2n(DMA)$ (**1**) is selected as an example here. In **1**, one C atom and one N atom from one coordinated DMA display positional disorder, and the relative ratio for C22−C30/N4−N6 is refined to 0.667/0.333. A large amount of spatially delocalized electron density in the lattice is found from which half dissociated DMA solvent could be identified. However, the remaining electron density is highly disordered, and it is quite hard to locate and refine other DMA molecules. Therefore, the final numbers of the solvent are confirmed by element analyses and TGA. The structural unit of **1** consists of two seven-coordinated Sm^{III} cations, three $azdc^{2-}$ ligands, and two coordinated DMA molecules (Figure 1a). The seven-coordinated Sm adopts monocapped trigonal prism geometry (Figure 1b), which is defined by six O from six H_2azdc ligands and one O from one DMA molecule with Sm−O distances 2.340(4)−2.499(4) Å (Figure 1c). Meanwhile, the evaluation of the polyhedral shape of Sm1 is executed by freely available program SHAPE.[13] The geometry around Sm1 indicates that its proximate ideal geometry is capped trigonal prism (CTPR) (Supporting Information Table S3). In the coordination polyhedron around Sm1, the O1, O4, O5 group and O2, O3, O7 group compose the two bottom surfaces of the trigonal prism with the dihedral angle of 12.6° for the two bottom planes. The distances of the Sm1 and the two bottom planes are 1.6049 and 1.6104 Å, respectively. The O1, O4, O2, O7 group, O1, O5, O3, O7 group, and O4, O5, O3, O2 group constitute the three side planes of the trigonal prism, and their standard deviations from their least-squares are 0.1256, 0.0961, and 0.0746 Å, respectively. The distances between Sm1 and the three side planes are 0.8933, 1.1951, and 0.5381 Å, respectively. Additionally, O6 locates the cap position covering the side plane defined by the O4, O5, O3, O2 group, and the distance between O6 and the plane is 1.9597 Å.

Interestingly, adjacent Sm1 cations are connected through six bridging tetradentate carboxylate groups to generate the 1D $[Sm_2(CO_2)_6]_n$ chain (Figure 1d), which further constructs the 3D frameworks (Figure 1e). To better understand the whole structure of **1**, the topological structure of **1** can be analyzed by the freely available program TOPOS.[14] If the H_2azdc ligands are regarded as linkers and Sm1 cations act as 6-connected node, the 3D framework of **1** can be depicted as a (4, 4, 6)-connected network with the Schläfli symbol of $\{4^2{\cdot}8^4\}\{4^4{\cdot}6^2\}_2$ $\{4^8{\cdot}6^6{\cdot}8\}_2$ (Figure 2), which corresponds to "fsy"-type topology that is rare for 3D CPs.[14]

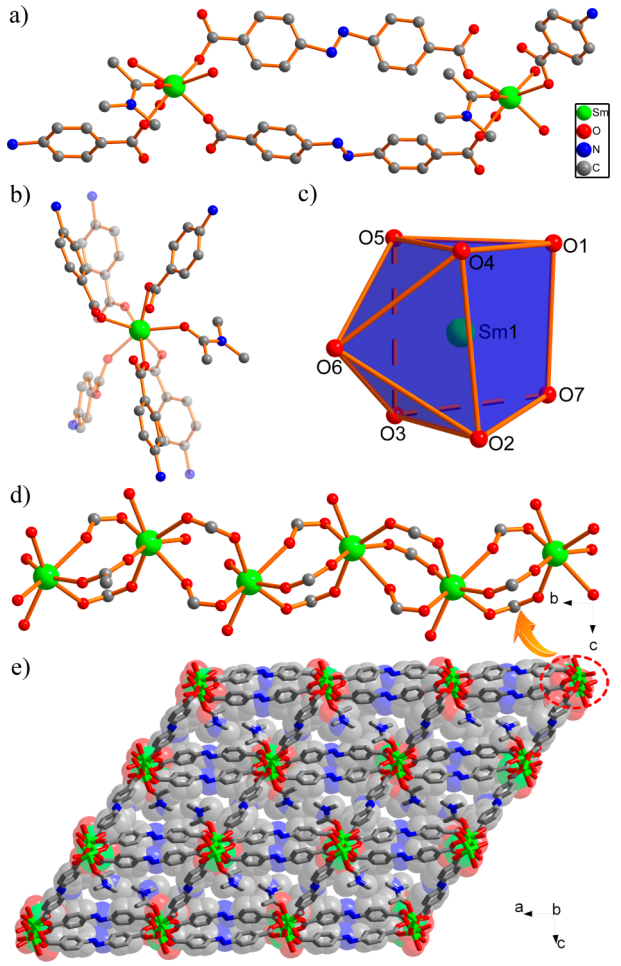

Figure 1. (a) Ball and stick representation of the molecular unit of **1**. (b, c) The coordination environment of the Sm^{III} cation. (d) The 1D chain-shaped building units $[Sm_2(CO_2)_6]_n$ constructed from the adjacent Sm^{III} cations and carboxyl groups of the H_2azdc ligands. (e) The 3D framework of **1**. H atoms and free DMA molecules are omitted for clarity.

It is worth noting that there are obvious distinctions between **1**, $[Tb_2(azdc)_3(DMSO)_4{\cdot}16(DMSO)]_n$ (**A**), $[Ce_3(azdc)_3(Hazdc)_3{\cdot}30(DMSO){\cdot}29(H_2O)]_n$ (**B**), and $[Ce_2(azdc)_3(H_2O)_3]_n$ (**C**). Compared with **A**,[1c] several significant differences are noticed in **1**: (i) Compound **1** was isolated by solvothermal methods rather than diffusion methods. (ii) The Sm^{III} cation in **1** is defined by seven O atoms from six H_2azdc ligands and one DMA molecule, whereas the Tb^{III} cation in **A**[1c] is defined by eight O atoms from five H_2azdc ligands and two DMSO molecules (Supporting Information Figure S2a). (iii) H_2azdc in **1** adopts the bridging mode and is bound to Sm^{III} cations to form the 3D noninterpenetrating framework with "fsy"-type topology. On the contrary, H_2azdc in **A**[1c] displays the bridging/chelating modes and links Tb^{III} cations to form the 3D interpenetrating structure with "pcu"-type topology (Supporting Information Figure S2b). Likewise, the remarkable differences among **1**, **B**,[2d] and **C**[2d] are clearly found: (i) Both **B**[2d] and **C**[2d] were obtained by diffusion methods. (ii) Two crystallographic unique Ce^{III} cations in **B**[2d] are 12-coordinated icosahedra of Ce1 and nine-coordinated tricapped trigonal prism of Ce2, respectively (Supporting Information Figure

dx.doi.org/10.1021/ic501395p | Inorg. Chem. 2014, 53, 10340−10346

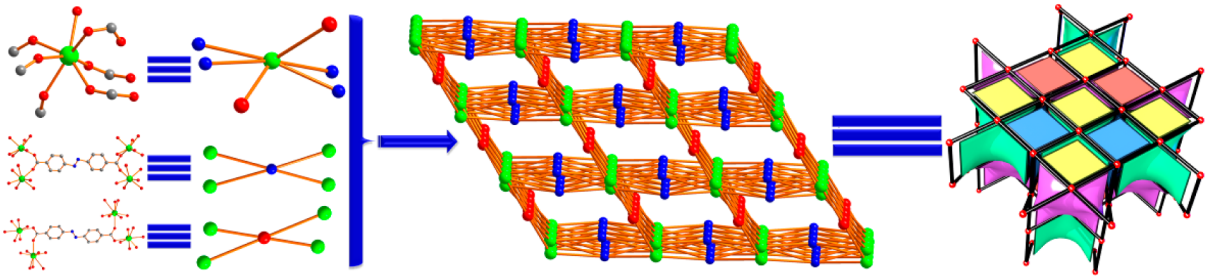

Figure 2. (Left and center) Schematic view of the (4,4,6)-connected net or "fsy"-type topology framework exhibited by **1**. (Right) The tiling.

S3a,b). Analogously, eight-coordinated Ce1 and nine-coordinated Ce2 coexist in $\mathbf{C}^{2d}$ (Supporting Information Figure S3d,e). (iii) $\mathbf{B}^{2d}$ presents a "NaCl"-type 3D network with an open channel (Supporting Information Figure S3c), whereas $\mathbf{C}^{2d}$ shows the 3D framework constructed from infinite chain-like SBUs (Supporting Information Figure S3f).

UV–Vis Spectra and Photoluminescence Properties. The room temperature solid state UV–vis spectra of **1**–**7** display three broad absorption bands centered at ca. 289, 382, and 473 nm, respectively (Suporting Information Figure S4). The observed main peak at ca. 473 nm might be attributed to the electronic transition between the highest occupied molecular orbital and the lowest unoccupied molecular orbital of H_2azdc. Similar phenomena have been encountered earlier for CPs synthesized with azo groups.[15] The additional bands at ca. 289 and 382 nm may be ascribed to the intraligand transitions. In contrast, the UV–vis spectrum of the free H_2azdc ligand displays three analogous broad bands at ca. 276, 347, and 467 nm, respectively (Supporting Information Figure S4). Note that three absorption bands in **1**–**7** obviously red-shift relative to that of the free H_2azdc ligand when coordinated to Ln^{III} cation, which can be ascribed to the coordination effect between the H_2azdc ligand and Ln^{III} cations. Meantime, the solid state photoluminescence property of **2** was selected as an example to carry out on powered sample at ambient temperature (Supporting Information Figure S5). The expected emission signals deriving from the vibronic character of the Eu^{III} cation were not detected and were hidden by the emission spectrum of the organic ligands containing azo functional groups in the region 400–700 nm; such a phenomenon has also been encountered in a uranyl–organic framework-type CP containing the H_2azdc ligand.[16]

TG Analyses and Variable-Temperature in Situ PXRD. The thermal stabilities were studied on the crystalline samples under the N_2 atmosphere for **1**–**7** from 25 to 800 °C (Supporting Information Figure S6). All the TG curves are very similar and display a unique weight loss taking place between 100 and 500 °C, related to the release of DMA. Expected weight losses are in good accordance with the calculated one based on the stoichiometric chemical formulas. In the case of **1**, the weight loss value is 24.45% (calcd 23.97%). For **2**, the weight loss value is 24.38% (calcd 23.92%). For **3**, the weight loss value is 23.19% (calcd 23.74%). As for **4**, the weight loss value is 23.40% (calcd 23.70%). For **5**, the weight loss value is 23.45% (calcd 23.58%). For **6**, the weight loss value is 22.89% (calcd 23.50%). For **7**, the weight loss value is 22.76% (calcd 23.42%).

In addition, since CPs **1**–**7** exhibit similar thermal behavior, the variable-temperature in situ PXRD pattern for **1** as an example has also been examined on a Pt sample platform under N_2 atmosphere from 25 to 550 °C (Figure 3). The

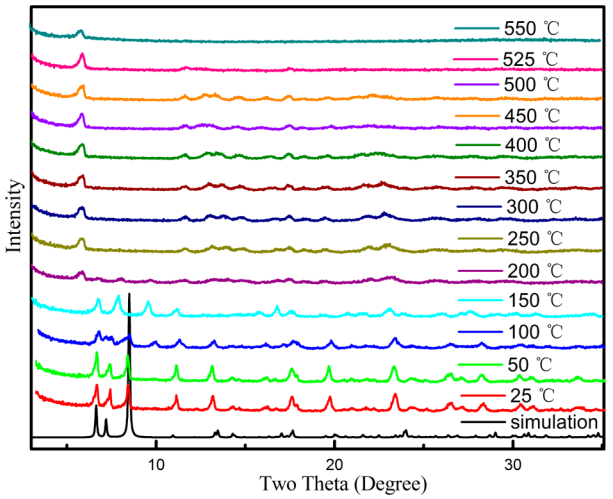

Figure 3. In situ variable-temperature PXRD pattern for **1**, measured on a Pt sample platform under N_2 atmosphere in the range 25–550 °C.

corresponding PXRD patterns determine that the structure of **1** is unchanged when heated to 100 °C. As the temperature increases to 200 °C, the peaks appearing at ca. 3–10° start to shift, which is assumed as the release of two free DMA molecules. Nevertheless, from 200 to 500 °C, the peaks present at ca. 6.7°, 7.2°, and 8.5° begin to decrease gradually and disappear finally. Correspondingly, a new peak at ca. 5.9° turns up, and the weight loss corresponds to the removal of two coordinated DMA molecules; however, the patterns indicate that **1** is still crystalline. Upon further heating, the diffraction peaks are barely noticeable, indicating that the framework in **1** sets out to collapse and **1** becomes amorphous. Moreover, the results are consistent with the TG analyses.

Magnetic Properties. Since 2003, and especially in the last five years, SMMs based on CPs of f-elements have attracted much interest in molecular magnetism.[3,17] According to the structural analyses discussed above, each COO^- carboxylate group in **1**–**7** connects two Ln^{III} cations; as a result, it is necessary to study magnetic properties and assess the eventual exchange interactions between adjacent Ln^{III} cations.

The temperature dependence of the magnetic susceptibilities of **1**–**7** are recorded in the range 1.8–300 K at 1000 Oe, as depicted in Figure 4. The field dependence data of magnetization measurements at 2 K for **1**–**7** are also examined (Supporting Information Figure S7).

For **3**, $\chi_M T$ is 15.81 cm^3 K mol^{-1} at 300 K, consistent with the expected value of two free Gd^{III} ions (15.76 cm^3 K mol^{-1}, $^8S_{7/2}$, $g = 2$).[18] As the temperature is decreased, $\chi_M T$ increases and almost keeps constant until ca. 50 K, and then increases

dx.doi.org/10.1021/ic501395p | Inorg. Chem. 2014, 53, 10340–10346

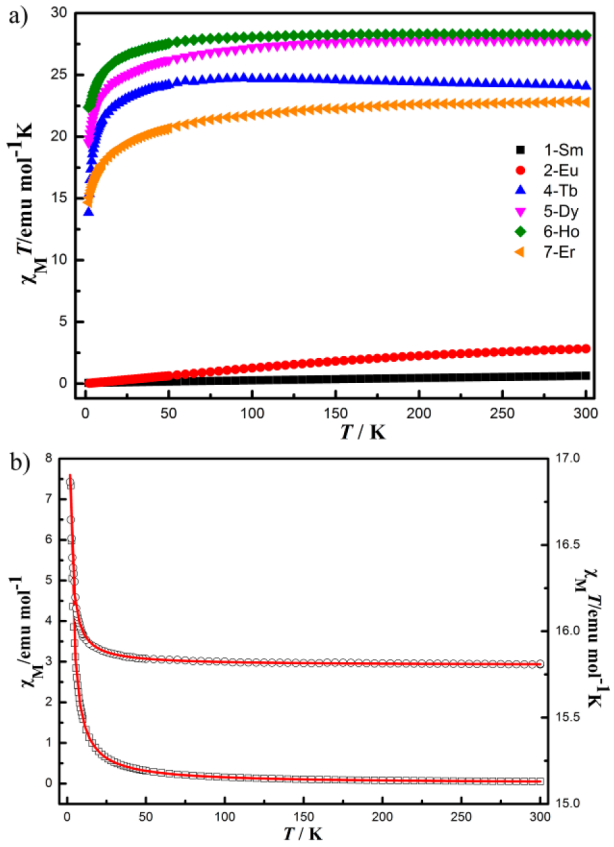

Figure 4. Temperature dependence of magnetic susceptibilities in the form of $\chi_M T$ vs T for **1**−**7** at 1000 Oe between 1.8 and 300 K: **1**, **2**−**7** (a), **3** (b).

rapidly on further cooling, reaching a maximum of 16.87 cm^3 K mol^{-1} at 1.8 K (Figure 4b), suggesting a ferromagnetic interactions between adjacent Gd^{III} ions.

As described in the crystal structures part, adjacent Gd^{III} ions are bridged by COO$^-$ groups to give a $[Gd_2(CO_2)_6]_n$ chain in **3**, and the nearest Gd^{III}···Gd^{III} distance is 4.636(4) Å, much shorter than the distance between adjacent 1D chains (longer than 12 Å). Therefore, the magnetic interaction between adjacent 1D chains can be neglected to simplify the 1D chain model. The expression deduced by Fisher[19] (eq 1) could be applied for quantitatively analysis the interaction between adjacent Gd^{III} ions.

$$\chi_{chain} = \frac{Ng^2\beta^2}{3kT}\frac{S(S+1)(1+u)}{1-u} \quad (1)$$

$$u = \coth(JS(S+1)/kT) - kT/(JS(S+1))$$

In eq 1, N is Avogadro's number, β is the Bohr magnetron, k is the Boltzmann constant, and J is the exchange coupling parameter between adjacent Gd^{III} cations. The best least-squares fit parameters are g = 2.003, J = 0.008 cm^{-1}, and $R = \sum[(\chi_M T)_{obsd} - (\chi_M T)_{calcd}]^2/\sum[(\chi_M T)_{obsd}]^2 = 2.018 \times 10^{-4}$. The magnitude of J is small but in the same order as other Gd^{III} complexes.[18b−h] The maximum of $\chi_M T$ is slightly higher than the value at 300 K, indicative of weak ferromagnetic coupling. Moreover, the curve of χ_M^{-1} vs T in 1.8−300 K obeys the Curie−Weiss law with C = 15.83 cm^3 K mol^{-1} and θ = 0.16 K (Supporting Information Figure S8), further supporting the occurrence of a weak ferromagnetic coupling between adjacent Gd^{III} ions in **3**.

It is noteworthy that the ferromagnetic interaction in **3** is more interesting in molecular magnetism. Literature examples on ferromagnetic interaction in Gd^{III} complexes only bridged by $\mu_{1,3}$-COO groups are rare, though several Gd^{III} complexes with ferromagnetic interaction linked by the same O atom of a carboxylate group have been documented.[18b−h] In **3**, the ferromagnetic interaction might be attributed to the accidental orthogonality between the magnetic orbits of adjacent Gd^{III} cations with suitable bridging angles and Gd^{III}···Gd^{III} distances, in accordance with the ranges of bridging angles and distances of the previous studies.[18b−h] Moreover, *ab initio* studies applied to Gd^{III} complexes manifest that ferromagnetic interactions between the Gd^{III} ions can also originate from the spin polarization effect through the monatomic oxygen and formate bridges.[20]

The magnetization data of **3** are carried out at a field 0.5−7 T between 2 and 10 K (Figure 5a), exhibiting a steady increase

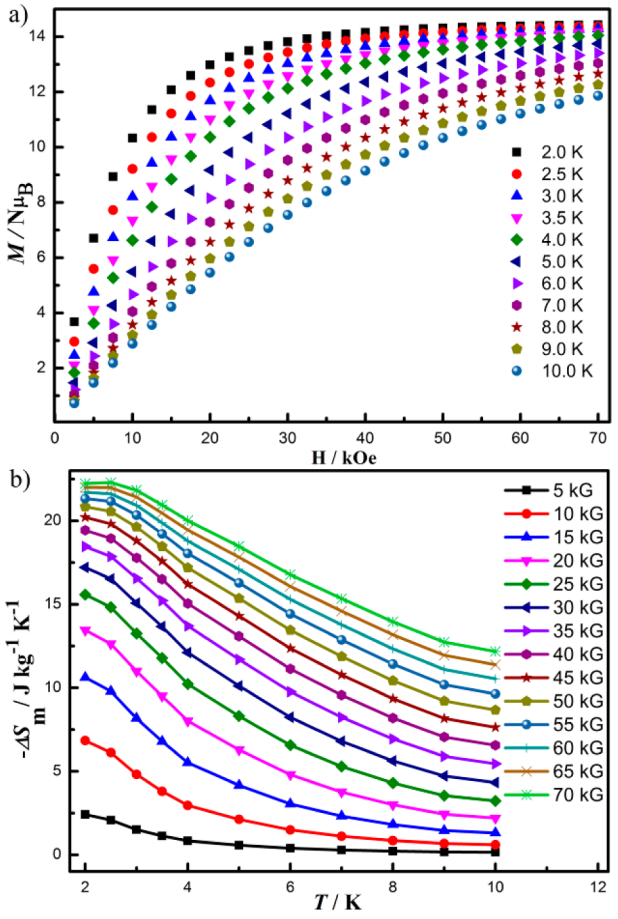

Figure 5. (a) Field dependencies of isothermal normalized magnetizations for **3** at T = 2−10 K and 0.5−7 T. (b) Temperature dependencies of magnetic entropy change ($-\Delta S_m$) as calculated from the magnetization data of **3** at T = 2−10 K and 0.5−7 T.

with increasing H and the saturation values of 13.98 $N\mu_B$ at 7 T and 2 K, being extremely approximate the theoretical value of 14 $N\mu_B$ for two individual Gd^{III} ($S = {}^7/_2$, g = 2) ions. The magnetic entropy change ΔS_m of **3** is calculated from the magnetization data by using the following Maxwell equation:[21]

$$\Delta S_m(T) = \int [\partial M(T, H)/\partial T]_H \, dH \quad (2)$$

dx.doi.org/10.1021/ic501395p | *Inorg. Chem.* 2014, 53, 10340−10346

In theory, the full entropy change per mole of **3** according to two Gd^{III} ions is 34.58 J mol^{-1} K^{-1}, calculated from $2R\ln(2S+1)$. Thus, the expected value of entropy change of **3** is 23.56 J kg^{-1} K^{-1}. The $-\Delta S_m$ value calculated by magnetizations is 22.29 J kg^{-1} K^{-1} at 2 K for ΔH = 7 T, equivalent to 34.86 mJ cm^{-1} K^{-1} (Figure 5b). The difference between the theoretical and experimental values may be ascribed to the M_W/N_{Gd} ratio of 734 (where molecular mass is M_W = 1467.65 g mol^{-1} and N_{Gd} is the number of Gd^{III} ions present per mole of **3**). The observed $-\Delta S_m$ is smaller than that of reported Gd^{III}-based molecular systems,[3b] close to the Gd-based polynuclear complex, 23 J kg^{-1} K^{-1} for $\{Gd_7\}$ (ΔH = 7 T at 3 K),[18i] however, significantly larger than the antiferromagnetic $\{Gd_2\}$ complex (17.25 J kg^{-1} K^{-1}, ΔH = 7 T at 3 K).[18j] The weak ferromagnetically coupled system could be favorable for magnetic cooling because of the combination of the advantages of low-lying excited states with ease of magnetization. Another recent interesting example is the $\{Cu_5Gd_4\}$ cluster reported by Murray.[22]

For **1**, **2**, **4**−**7**, $\chi_M T$ values at 300 K are 0.64 (**1**), 2.83 (**2**), 24.09 (**4**), 27.83 (**5**), 28.21 (**6**), and 22.88 (**7**) cm^3 K mol^{-1}, respectively (Figure 4a); the theoretical values for two isolated Ln^{III} cations follow: two Sm^{III} ($^6H_{5/2}$, $g = {}^2/_7$) are 0.18 cm^3 K mol^{-1} for **1**; two Eu^{III} ($^7F_0$, g = 0) are 0 cm^3 K mol^{-1} for **2**; two Tb^{III} ($^7F_6$, $g = {}^3/_2$) are 23.64 cm^3 K mol^{-1} for **4**; two Dy^{III} ($^6H_{15/2}$, $g = {}^4/_3$) are 28.34 cm^3 K mol^{-1} for **5**; two Ho^{III} ($^5I_8$, $g = {}^5/_4$) are 28.14 cm^3 K mol^{-1} for **6**; two Er^{III} ($^4I_{15/2}$, $g = {}^6/_5$) are 22.96 cm^3 K mol^{-1} for **7**.[18a]

When the temperature is lowered, $\chi_M T$ values of **1** and **2** decrease rapidly to 0.06 and 0.03 cm^3 K mol^{-1} at 1.8 K, respectively. The thermal variations of $\chi_M T$ are almost constant over the whole temperature range, being similar to those of previous reports.[18a] In the cases of **4**−**7**, $\chi_M T$ values decrease slowly from 300 to 40 K, then decrease distinctly to reach the minimum of 13.85, 19.53, 22.38, and 14.67 cm^3 K mol^{-1} at 1.8 K, respectively. In addition, the curves of $\chi_M{}^{-1}$ versus T in 1.8−300 K of **4**−**7** follow the Curie−Weiss law with negative θ values, resulting from the depopulation of Stark sublevels (Supporting Information Figure S9).

The field-dependent magnetizations (M) for **1**, **2**, **4**−**7** have been measured at 2 K in the range 0−7 T (Supporting Information Figure S7). The M values of **1** and **2** increase linearly and reach 0.22 and 0.16 $N\mu_B$, respectively. While the M values of **3**−**7** increase dramatically with increasing field at low fields, they subsequently linearly increase at higher fields reaching the values of 13.98, 11.12, 10.85, 10.81, and 10.69 $N\mu_B$, respectively. These values are much lower than the expected values for non interacting Ln^{III} cations, demonstrating the presence of anisotropy and significant crystal field effects.[16c,23]

To further study the magnetic dynamics, temperature-dependent alternating-current (ac) magnetic susceptibilities for **3**, **4**, and **5** are measured at zero direct-current (dc) fields (Figure 6a and Supporting Information Figure S10). For **3** and **4**, no out-of-phase signal is detected. In contrast, in the case of **5**, both in-phase (χ_M') and out-of-phase (χ_M'') components of the susceptibilities exhibit frequency-dependent behavior below ca. 8 K, indicative of the presence of slow magnetic relaxation. Unfortunately, no peak of χ_M'' is detected, which is usually encountered in Dy^{III} complexes.[3a] Therefore, the energy barrier of **5** could not be gained by Arrhenius fitting. Assuming that only one relaxation process exists in **5**, the energy barrier (E_a)

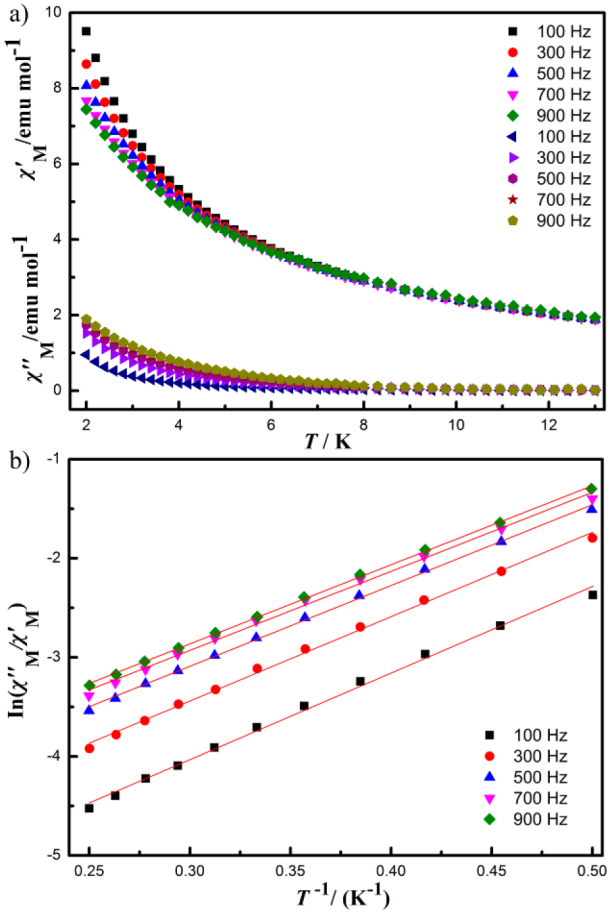

Figure 6. (a) Temperature dependence of in-phase (χ_M') and out-of-phase (χ_M'') ac susceptibility components at different frequencies for **5** with zero dc field and an oscillation of 3 Oe. (b) Plots of natural logarithm of χ''_M/χ'_M versus $1/T$ for **5**, the solid lines represent the fitting results over the range of 100−900 Hz.

could be roughly estimated with the following equation (eq 3):[24]

$$\ln(\chi''_M/\chi'_M) = \ln(\omega\tau_0) + E_a/k_BT \quad (3)$$

As depicted in Figure 6b, by fitting the experimental χ''_M/χ'_M data to eq 3, we obtained an estimation of the energy barrier $E_a/k_B \approx 8.30$ K (8.74, 8.65, 8.16, 7.89, 8.07 K for 100, 300, 500, 700, 900 Hz) and $\tau_0 \approx 8.37 \times 10^{-6}$ s (1.29×10^{-5}, 8.31×10^{-6}, 7.88×10^{-6}, 6.97×10^{-6}, 5.79×10^{-6} for 100, 300, 500, 700, 900 Hz), which are in the normal range 10^{-6}−10^{-11} s for SMMs.[3a]

CONCLUSIONS

In conclusion, a series of 3D Ln-CPs with H_2azdc have been successfully prepared via solvothermal method. CPs **1**−**7** all construct by 1D $[Ln_2(CO_2)_6]_n$ building units, further generating the 3D (4, 4, 6)-net frameworks with the Schläfli symbol of $\{4^2{\cdot}8^4\}\{4^4{\cdot}6^2\}_2\{4^8{\cdot}6^6{\cdot}8\}_2$. The magnetic characterization reveals that CP **3** displays cryogenic magnetic refrigeration property and CP **5** exhibits slow magnetic relaxation. It should be noticed that the successful preparation of **1**−**7** not only demonstrates that the hydrothermal method is an effective strategy in preparing high-dimensional CPs, but also enriches the structural variety of Ln-CPs. More novel Ln-CPs with interesting properties would be discovered by

dx.doi.org/10.1021/ic501395p | Inorg. Chem. 2014, 53, 10340−10346

replacing other organic polycarboxylic ligands in the following period.

■ ASSOCIATED CONTENT

Supporting Information

PXRD patterns, TGA data, spectroscopic characterizations, and magnetic and crystallographic data of CPs **1**−**7**, including data in CIF format. This material is available free of charge via the Internet at http://pubs.acs.org.

■ AUTHOR INFORMATION

Corresponding Authors

*E-mail: shiwei@nankai.edu.cn. Fax: (+86) 22-23502458.
*E-mail: pcheng@nankai.edu.cn. Fax: (+86) 22-23502458.

Notes

The authors declare no competing financial interest.

■ ACKNOWLEDGMENTS

This work was supported by the MOST ("973 program" 2012CB821702), the NSFC (21331003), the MOE (IRT-13R30), 111 project (B12015), and the NSF of Tianjin (13JCZDJC32200).

■ REFERENCES

(1) (a) Pan, L.; Huang, X. Y.; Li, J.; Wu, Y. G.; Zheng, N. W. *Angew. Chem., Int. Ed.* **2000**, *39*, 527. (b) Johnson, A. M.; Young, M. C.; Zhang, X.; Julian, R. R.; Hooley, R. J. *J. Am. Chem. Soc.* **2013**, *135*, 17723. (c) Reineke, T. M.; Eddaoudi, M.; Moler, D.; O'Keeffe, M.; Yaghi, O. M. *J. Am. Chem. Soc.* **2000**, *122*, 4843. (d) Tranchemontagne, D. J.; Mendoza -Cortés, J. L.; O'Keeffe, M.; Yaghi, O. M. *Chem. Soc. Rev.* **2009**, *38*, 1257.

(2) (a) Feng, J.; Zhang, H. J. *Chem. Soc. Rev.* **2013**, *42*, 387. (b) Heffern, M. C.; Matosziuk, L. M.; Meade, T. J. *Chem. Rev.* **2014**, *114*, 4496. (c) Cui, Y. J.; Yue, Y. F.; Qian, G. D.; Chen, B. L. *Chem. Rev.* **2012**, *112*, 1126. (d) Han, Y. F.; Li, X. Y.; Li, L. Q.; Ma, C. L.; Shen, Z.; Song, Y.; You, X. Z. *Inorg. Chem.* **2010**, *49*, 10781.

(3) (a) Woodruff, D. N.; Winpenny, R. E. P.; Layfield, R. A. *Chem. Rev.* **2013**, *113*, 5110. (b) Zheng, Y. Z.; Zhou, G. J.; Zheng, Z. P.; Winpenny, R. E. P. *Chem. Soc. Rev.* **2014**, *43*, 1462.

(4) Ghiassi, K. B.; Olmstead, M. M.; Balch, A. L. *Dalton Trans.* **2014**, *43*, 7346.

(5) (a) Li, H. H.; Shi, W.; Zhao, K. N.; Niu, Z.; Li, H. M.; Cheng, P. *Chem.—Eur. J.* **2013**, *19*, 3358. (b) Shi, P. F.; Zheng, Y. Z.; Zhao, X. Q.; Xiong, G.; Zhao, B.; Wan, F. F.; Cheng, P. *Chem.—Eur. J.* **2012**, *18*, 15086. (c) Xia, J.; Zhao, B.; Wang, H. S.; Shi, W.; Ma, Y.; Song, H. B.; Cheng, P.; Liao, D. Z.; Yan, S. P. *Inorg. Chem.* **2007**, *46*, 3450. (d) Zhou, J. M.; Shi, W.; Xu, N.; Cheng, P. *Inorg. Chem.* **2013**, *52*, 8082. (e) Han, T.; Shi, W.; Niu, Z.; Na, B.; Cheng, P. *Chem.—Eur. J.* **2013**, *19*, 994. (f) Han, T.; Shi, W.; Zhang, X. P.; Li, L. L.; Cheng, P. *Inorg. Chem.* **2012**, *51*, 13009. (g) Chen, Z.; Zhao, B.; Cheng, P.; Zhao, X. Q.; Shi, W.; Song, Y. *Inorg. Chem.* **2009**, *48*, 3493. (h) Zhang, Z. J.; Zhang, S. Y.; Li, Y.; Niu, Z.; Shi, W.; Cheng, P. *CrystEngComm* **2010**, *12*, 1809.

(6) Kumar, G. S.; Neckers, D. C. *Chem. Rev.* **1989**, *89*, 1915.

(7) (a) Lyndon, R.; Konstas, K.; Ladeig, B. P.; Southon, P. D.; Kepert, C. J.; Hill, M. R. *Angew. Chem., Int. Ed.* **2013**, *52*, 3695. (b) Li, T.; Kozlowski, M. T.; Doud, E. A.; Blakely, M. N.; Rosi, N. L. *J. Am. Chem. Soc.* **2013**, *135*, 11688. (c) Furukawa, H.; Kim, J.; Ockwig, N. W.; O'Keeffe, M.; Yaghi, O. M. *J. Am. Chem. Soc.* **2008**, *130*, 11650. (d) Gu, X. J.; Lu, Z. H.; Xu, Q. *Chem. Commun.* **2010**, *46*, 7400. (e) Chen, B. L.; Ma, S. Q.; Hurtado, E. J.; Lobkovsky, E. B.; Zhou, H. C. *Inorg. Chem.* **2007**, *46*, 8490. (f) Guo, J. S.; Xu, G.; Guo, G. C.; Huang, J. S. *Cryst. Growth Des.* **2013**, *13*, 2642. (g) Yadav, P. K.; Kumari, N.; Pachfule, P.; Banerjee, R.; Mishra, L. *Cryst. Growth Des.* **2012**, *12*, 5311. (h) Bhattacharya, S.; Sanyal, U.; Natarajan, S. *Cryst. Growth Des.* **2011**, *11*, 735. (i) Hou, Y. F.; Yu, Y.; Yue, K. F.; Wei, Q.; Liu, Y. L.; Zhou, C. S.; Wang, Y. Y. *CrystEngComm* **2013**, *15*, 7161. (j) Volkringer, C.; Loiseau, T.; Devic, T.; Férey, G.; Popov, D.; Burghammer, M.; Riekel, C. *CrystEngComm* **2010**, *12*, 3225. (k) Chen, Z. F.; Zhang, Z. L.; Tan, Y. H.; Tang, Y. Z.; Fun, H. K.; Zhou, Z. Y.; Abrahams, B. F.; Liang, H. *CrystEngComm* **2008**, *10*, 217. (l) Liu, Y. L.; Yue, K. F.; Shan, B. H.; Xu, L. L.; Wang, C. J.; Wang, Y. Y. *Inorg. Chem. Commun.* **2010**, *13*, 388. (m) Fu, F.; Li, D. S.; Yang, X. G.; Zhang, C. Q.; Wu, Y. P.; Zhao, J.; Wang, E. B. *Inorg. Chem. Commun.* **2009**, *12*, 657.

(8) Lin, X.; Liu, T. F.; Lin, J. X.; Yang, H. X.; Lü, J.; Xu, B.; Cao, R. *Inorg. Chem. Commun.* **2010**, *13*, 388.

(9) Ameerunisha, S.; Zacharias, P. S. *J. Chem. Soc., Perkin Trans.* **1995**, *2*, 1679.

(10) (a) Sheldrick, G. M. *SHELXS97, Program for Crystal Structure Solution*; University of Göttingen: Göttingen, Germany, 1997. (b) Sheldrick, G. M. *SHELXL97, Program for Crystal Structure Refinement*; University of Göttingen: Göttingen, Germany, 1997.

(11) (a) Brown, I. D.; Altermatt, D. *Acta Crystallogr.* **1985**, *B41*, 244−247. (b) Brese, N. E.; O'Keeffe, M. *Acta Crystallogr.* **1991**, *B47*, 192−197. (c) O'Keeffe, M.; Brese, N. E. *Acta Crystallogr.* **1992**, *B48*, 152−154.

(12) (a) Zhang, S. W.; Wang, Y.; Zhao, J. W.; Ma, P. T.; Wang, J. P.; Niu, J. Y. *Dalton Trans.* **2012**, *41*, 3764−3772. (b) Zhang, S. W.; Zhao, J. W.; Ma, P. T.; Chen, H. N.; Niu, J. Y.; Wang, J. P. *Cryst. Growth Des.* **2012**, *12*, 1263.

(13) (a) *SHAPE, version 2.0; Continuous Shape Measures Calculation*; Electronic Structure Group, Universiat de Barcelona: Barcelona, Spain, 2010. (b) Casanova, D.; Liunell, M.; Alemany, P.; Alvarez, S. *Chem.—Eur. J.* **2005**, *11*, 1479.

(14) (a) Blatov, V. A.; Shevchenko A. P.; Serezhkin, V. N. *J. Appl. Crystallogr.* **2000**, *33*, 1193. TOPOS software available at http://www.topos.ssu.samara.ru. (b) O'Keeffe, M.; Yaghi O. M.; Ramsden, S. *Reticular Chemistry Structure Resource*; 2007, database available at http://rcsr.anu.edu.au/.

(15) (a) Fliegl, H.; Kohn, A.; Hattig, C.; Ahlrichs, R. *J. Am. Chem. Soc.* **2003**, *125*, 9821. (b) Bhattacharya, S.; Sanyal, U.; Natarajan, S. *Cryst. Growth Des.* **2011**, *11*, 735.

(16) Mihalcea, I.; Henry, N.; Bousquet, T.; Volkringer, C.; Loiseau, T. *Cryst. Growth Des.* **2012**, *12*, 4641.

(17) Benelli, C.; Gatteschi, D. *Chem. Rev.* **2002**, *102*, 2369.

(18) (a) Aguilàm, D.; Barrios, L. A.; Velasco, V.; Arnedo, L.; Aliaga-Alcalde, N.; Menelaou, M.; Teat, S. J.; Roubeau, O.; Luis, F.; Aromí, G. *Chem.—Eur. J.* **2013**, *19*, 5881. (b) Cañadillas-Delgado, L.; Pasán, J.; Fabelo, O.; Hernández-Molina, M.; Lloret, F.; Julve, M.; Ruiz-Pérez, C. *Inorg. Chem.* **2006**, *45*, 10585. (c) Hernández-Molina, M.; Ruiz-Pérez, C.; López, T.; Lloret, F.; Julve, M. *Inorg. Chem.* **2003**, *42*, 5456. (d) Xu, N.; Shi, W.; Liao, D. Z.; Yan, S. P.; Cheng, P. *Inorg. Chem.* **2008**, *47*, 8748. (e) Hou, H. W.; Li, G.; Li, L. K.; Zhu, Y.; Meng, X. R.; Fan, Y. T. *Inorg. Chem.* **2003**, *42*, 428. (f) Hatscher, S. T.; Urland, W. *Angew. Chem., Int. Ed.* **2003**, *42*, 2862. (g) Costes, J. P.; Clemente-Juan, J. M.; Dahan, F.; Nicodème, F.; Verelst, M. *Angew. Chem., Int. Ed.* **2002**, *41*, 323. (h) Baggio, R.; Calvo, R.; Garland, M. T.; Peña, O.; Perec, M.; Rizzi, A. *Inorg. Chem.* **2005**, *44*, 8979. (i) Sharples, J. W.; Zheng, Y. Z.; Tuna, F.; Mclnnes, E. J. L.; Collison, D. *Chem. Commun.* **2011**, *47*, 7650. (j) Biawas, S.; Jena, H. S.; Goswami, S.; Sanda, S.; Konar, S. *Cryst. Growth Des.* **2014**, *14*, 1287.

(19) Fisher, M. E. *Am. J. Phys.* **1964**, *32*, 343.

(20) Zhu, L.; Yao, K. L.; Liu, Z. L. *Phys. Rev. B* **2007**, *76*, 134409.

(21) (a) Torres, F.; Hernández, M.; Bohigas, X.; Tejada, J. *Appl. Phys. Lett.* **1964**, *32*, 343. (b) Evangelisti, M.; Luis, F.; de Jongh, L. J.; Affronte, M. *J. Mater. Chem.* **2006**, *16*, 2534. (c) Evangelisti, M.; Brechin, E. K. *Dalton Trans.* **2010**, *39*, 4672.

(22) Langley, S. K.; Chiton, N. F.; Moubaraki, B.; Hooper, T.; Brechin, E. K.; Evangelisti, M.; Murray, K. S. *Chem. Sci.* **2011**, *2*, 1166.

(23) Zhou, J. M.; Shi, W.; Xu, N.; Cheng, P. *Cryst. Growth Des.* **2013**, *13*, 1218.

(24) Nihei, M.; Okamoto, Y.; Sekine, Y.; Hoshino, N.; Shiga, T.; Liu, I. P. C.; Oshio, H. *Angew. Chem., Int. Ed.* **2012**, *51*, 6361.